crystals

MDPI

Article

Manufacturing and Thermal Shock Resistance of 3D-Printed Porous Black Zirconia for Concentrated Solar Applications

Fernando Almeida Costa Oliveira [1,*], Manuel Sardinha [2], José Galindo [3], José Rodríguez [3], Inmaculada Cañadas [3], Marco Leite [2] and Jorge Cruz Fernandes [2]

[1] LNEG—Laboratório Nacional de Energia e Geologia I.P., LEN—Laboratório de Energia, UME—Unidade de Materiais para a Energia, Estrada do Paço do Lumiar 22, 1649-038 Lisboa, Portugal
[2] IDMEC—Instituto de Engenharia Mecânica, Instituto Superior Técnico, University of Lisboa, Av. Rovisco Pais, 1049-001 Lisboa, Portugal; manuel.r.sardinha@tecnico.ulisboa.pt (M.S.); marcoleite@tecnico.ulisboa.pt (M.L.); cruz.fernandes@tecnico.ulisboa.pt (J.C.F.)
[3] CIEMAT—Centro de Investigaciones Energéticas, Medioambientales y Tecnológicas, PSA–Plataforma Solar de Almería, Apartado 22, E-04200 Tabernas, Almería, Spain; jose.galindo@psa.es (J.G.); jose.rodriguez@psa.es (J.R.); i.canadas@psa.es (I.C.)
* Correspondence: fernando.oliveira@lneg.pt; Tel.: +351-210924600

Abstract: A novel approach for manufacturing porous materials, foreseen as solar receivers for concentrated sun radiation, used in the power tower technology is presented. In such applications, materials are subjected to steep thermal gradients and thousands of cycles. Yet, materials consisting of honeycombs and ceramic foams showed insufficient thermal performance. By using the fused filament fabrication process, one can design printed parts meeting the requirements for solar receivers, namely dark color and high solar absorptance. This exploratory study unveils data on the retained crushing strength of newly developed 3D-printed porous Black Zirconia cubes after thermal cycling under similar conditions to those experienced by volumetric receivers and catalyst substrates for solar fuels (H_2 and/or CO) production via the thermochemical cycle. Unlike dense ceramics, the resistance to thermal shock of 3D-printed cubes underwent a gradual decrease with the increase in the thermal gradient. The thermal shock cycles were performed between 800 °C and 1100, 1200, and 1300 °C, corresponding to a ΔT of 300, 400, and 500 K, respectively. Additionally, water quenching tests were performed at ΔT = 300 K up to 400 K. Crushing strength measurements carried out to evaluate the retained mechanical strength after exposure up to 100 cycles showed that the Black Zirconia cubes can withstand thermal gradients up to at least 400 K.

Keywords: 3D printing; fused filament fabrication; black zirconia; thermal shock; crushing strength; solar receiver; additive manufacturing

Citation: Costa Oliveira, F.A.; Sardinha, M.; Galindo, J.; Rodríguez, J.; Cañadas, I.; Leite, M.; Fernandes, J.C. Manufacturing and Thermal Shock Resistance of 3D-Printed Porous Black Zirconia for Concentrated Solar Applications. *Crystals* **2023**, *13*, 1323. https://doi.org/10.3390/cryst13091323

Academic Editors: Tomasz Sadowski, Aliakbar Emdadi and Sabine Weiß

Received: 28 July 2023
Revised: 15 August 2023
Accepted: 27 August 2023
Published: 29 August 2023

1. Introduction

Technological development of key components for green electricity production in solar power tower plants requires high-temperature resistance materials capable of operating under stringent conditions for long periods. Several pilot–plant feasibility studies have shown that porous ceramics are attracting special attention among potential candidates. Typically, high-porosity materials, such as ceramic foams and honeycombs, are used in tower technology to convert solar concentrated radiation into heat [1–8]. A 2.5 MWth air receiver facility—jointly developed and operated by CIEMAT-PSA and Deutsches Zentrum für Luft- und Raumfahrt e.V., abbreviated DLR—consisting of an air recirculation loop and thermal storage, and a steam generator was assembled on the top of the CESA-1 tower in 1991 [9]. The volumetric receiver outlet temperature reached 700 °C with peak flux densities of 800 kW m^{-2} within 20 min after a cold start [10]. More recently, a 5 kW solar receiver prototype proved to deliver air flows at temperatures exceeding 1000 °C using 10 ppi (pores per inch) siliconized silicon carbide foams at the solar high flux solar

simulator of the Eidgenössische Technische Hochschule (ETH), Zürich, Switzerland [11]. However, few data are available in the open literature regarding the performance of such porous materials under direct exposure to concentrated solar beams. The present research work aims to evaluate the damage imposed on developed 3D-printed porous Black Zirconia under drastic thermal shock conditions, replicating those experienced by solar open volumetric air receivers. Unlike components made from white zirconia, using black zirconia is expected to improve the solar radiation absorptance of the exposed receivers. To this end, an experimental setup, developed in 2016 in collaboration with CIEMAT-PSA, was employed, which includes a guillotine system, a secondary concentrator (termed homogenizer), and a temperature control system, allowing the performance of thermal shock cycles, which cannot be achieved in conventional electrical or gas furnaces [12]. In this study, the thermal resistance of a new absorber was assessed by thermal cycling under well-established conditions using the renewed SF60 solar furnace with a power output of 60 kW. Commonly termed 3D printing, additive manufacturing (AM) is the diversity of computer-controlled technologies that create three-dimensional objects by superimposing materials layer by layer. These technologies are being employed in various application fields, such as tissue engineering, energy production, microfluidic components, and high strength-to-weigh applications [13–15]. Among the most acclaimed advantages of additive manufacturing (AM) technologies are their design flexibility, the ability to re-imagine and produce tailored functionalities and material arrangements, and the potential for waste minimization [16]. AM demonstrates high versatility in both its production capabilities and the range of process families it encompasses. Among all the available processes, fused filament fabrication (FFF) is regarded as one of the most accessible, variable, and cost-effective AM techniques for processing polymer and polymer composite materials [17,18]. In FFF, an extrusion head system is attached to a carriage, where a thermoplastic material is heated to a semi-molten state and selectively deposited onto a build platform [17,19].

Ceramics have high hardness and brittleness, making them difficult to machine without generating internal and surface defects [20]. Moreover, ceramic machining is commonly very expensive. According to Klocke's estimation [21], it can account for more than 70% of component costs. Ceramics made by AM are regarded as an alternative for producing geometrically complex structures of such brittle and challenging materials to work with [22]. Additively manufactured ceramics have been used to produce tailor-made parts for numerous applications, such as impellers for the aerospace sector, dental crowns and prosthetics for the medical field, or heat exchangers and thermal insulators for the energy sector [23,24]. Even so, there are still challenges to overcome, namely the optimization of processing parameters that guarantee high-density parts with few defects and adequate mechanical performance.

Several AM processes such as selective laser sintering, digital light processing, or binder jetting have been used to process ceramic parts, but the process simplicity of FFF of ceramic polymer materials has seen recent developments and has been gaining increased attention from both industry and academia [25,26].

Some of the limiting factors of FFF ceramics are related to geometrical defects and minimum feature size, as well as the need for prolonged thermal cycles to prevent defects, such as cracks and blisters, resulting from trapped pyrolysis products. The available literature on ceramics produced with FFF is mostly focused on the production stages of both alumina and zirconia parts and their mechanical properties [27–30]. To address these challenges, extensive research has been conducted on filament composition and preparation [31,32].

Reports on the mechanical characterization of FFF ceramics are still scarce, with component properties being very variable, which is common in newly developed FFF variants [33–35]. Cano et al. [36] evaluated the influence of infill orientation on both the generated defects and the three-point bending strength of FFF zirconia specimens. Among the identified defects affecting the results, pores within extrusion paths were correlated

with binder parameters, and the variability of extrusion width led to geometric defects in the final components.

The determination of the thermal shock resistance of advanced ceramics by water quenching is based on the rapid heat transfer of a test specimen at an elevated temperature in a distilled water bath at room temperature. The specimens are kept at a soaking temperature (ranging from 320 to 420 °C, in the present case) for 1 h before quenching, for comparison purposes. Damage was assessed by determining the retained crushing strength after quenching tests at various temperature differences, ΔT, which is defined as the soaking temperature of the test specimen minus the temperature of the bath, and is set at 20 °C. For quantitative purposes, a critical temperature interval (ΔT_c) is set when a reduction in the mean retained strength of at least 30% is recorded.

The goal of the present work was to determine the thermal shock resistance of 3D-printed cubes caused by cumulative damage imposed on the materials directly exposed to a concentrated solar beam. The thermal shock cycles were carried out at temperatures ranging from 800 °C to 1300 °C, corresponding to a maximum ΔT = 500 K. The effect of both ΔT and the number of cycles on the retained crushing strength will be discussed. The difference in thermal resistance between samples exposed to solar radiation and water quenched shall be highlighted. The results show that the developed 3D-printed cubes based on Black Zirconia can withstand thermal shock without considerable damage for ΔT up to 400 K for 50 cycles.

2. Materials and Methods

2.1. 3D Printing

The 3D-printed samples were obtained through FFF using the 3 mol% Y_2O_3-stabilized Zetamix Black Zirconia (YSZ) ceramic-based filament developed by Nanoe®. According to the manufacturer, it is composed of roughly 50 vol% of fine ceramic particles (<1.0 μm) dispersed into a thermoplastic-based binder. A noticeable difference between Black and White Zirconia is the cobalt iron oxide $(Co, Fe)_2O_4$ added to its chemical composition, giving the material a dark color. According to the material's manufacturer, Black Zirconia will display slightly lower mechanical strength when compared with its White counterpart, with the final ceramic bodies having a minimum bending strength of 400 MPa [37]. Its usability is more demanding in the 3D printing production stage than most FFF thermoplastic processing. There is still a scarcity of publicly available information on fabricating 3D-printed Black Zirconia parts, although detailed instructions and other properties of the filament can be found in its datasheet and production guidelines [38].

After printing the polymer ceramic mixture, the polymer binder must be removed, which involves two debinding steps. The first is a chemical debinding, which removes most of the polymeric mixture, and the second is a thermal debinding, which slowly removes the remaining polymer. For the chemical debinding, the green parts were immersed in an acetone bath at 40 °C for 2 h, as this process stage aims at removing most of the binding material, which corresponds to a weight loss of approximately 5% in weight after drying. The thermal debinding was then performed at around 500 °C, lasting up to 30 h. The production process was completed by sintering the green cubes in a $MoSi_2$ heating element electric furnace at 1500 °C with a holding time of 1.5 h using a heating rate equal to the cooling one set at 5 °C min^{-1} and reaching a total of 10 h. The scheme shown in Figure 1 highlights the steps required for producing Black Zirconia parts, from the modeling of the samples to the final sintering stage.

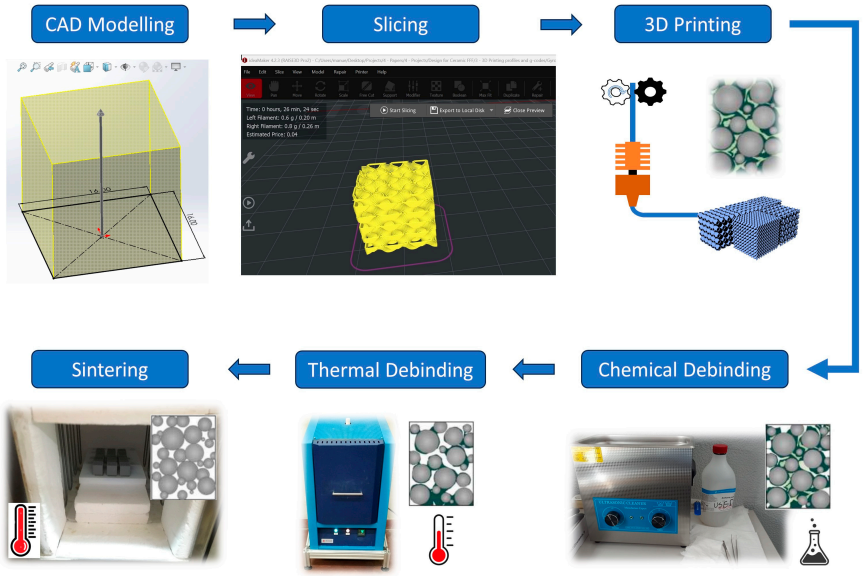

Figure 1. Scheme of the 3D-printing process used.

The machine used to produce the green cubes was a Raise3D dual extruder Pro 2 printer (Figure 2a). The machine has a direct drive extrusion system on which a wear-resistant nozzle was mounted. The slicer software used to prepare the print files was IdeaMaker 4.2.3.

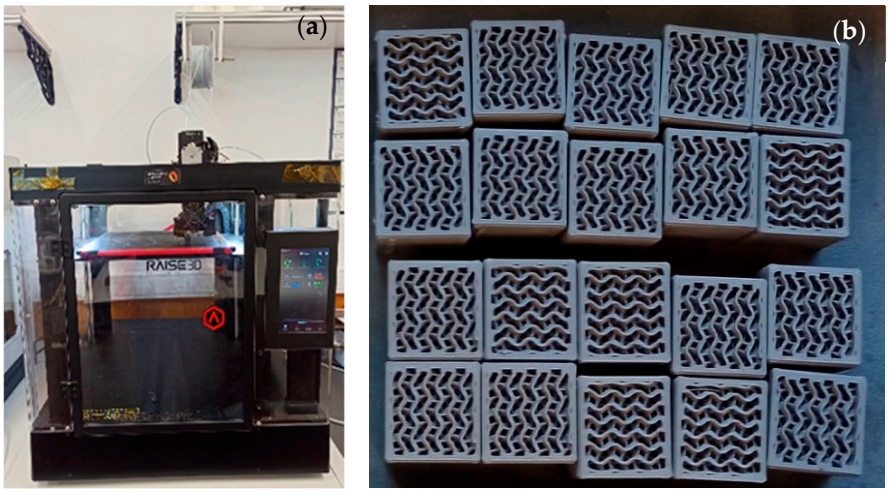

Figure 2. Raise3D Pro2 3D printer (**a**) and green parts after debinding (**b**).

Figure 2b shows the gyroid cuboid samples, produced by FFF, measuring 16.4 ± 0.4 mm on each side. The gyroid cellular structure, inspired by nature, which composes the final samples is obtained using the slicer software infill function. Specimens were made with a 25% gyroid infill with three perimeters and no top and bottom layers. The gyroid is a triply periodic minimal surface type structure. This geometry was selected due to its unique characteristics, such as both high surface area and specific mechanical properties, as well as the ability to divide space into continuous channels.

The geometric measurements of the cubes were performed using a Dino-Lite digital microscope coupled with DinoCapture 2.0 measurement software. For each case, samples were chosen and surface measurements in three different locations were taken, as can be seen in Figure 3a,b. Each dimension was measured 5 times.

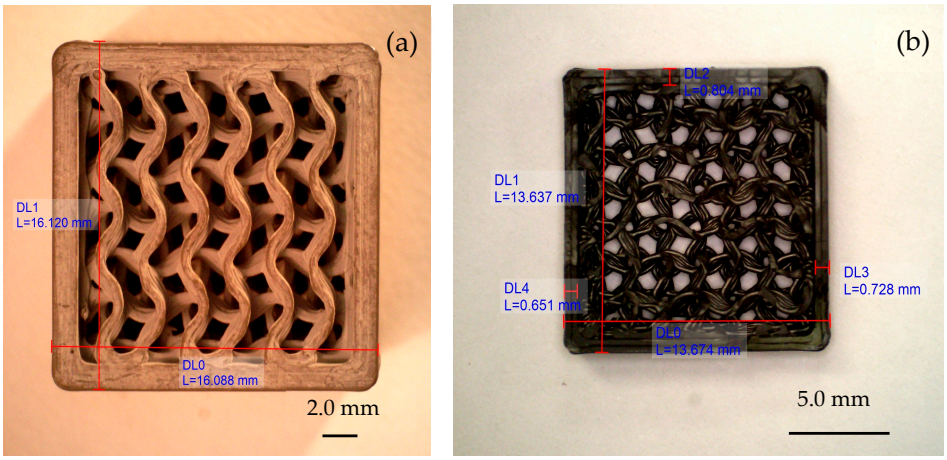

Figure 3. Top view of the cubes after printing (**a**) and sintering (**b**).

After sintering, the measured linear shrinkage was around 19% (Figure 4). For this reason, an equivalent scale factor was considered during the cubes' design and modeling stages of the components. After sintering, the measured mean value of the cube's edges was 13.1 ± 0.6 mm, and 38 cuboid samples were produced.

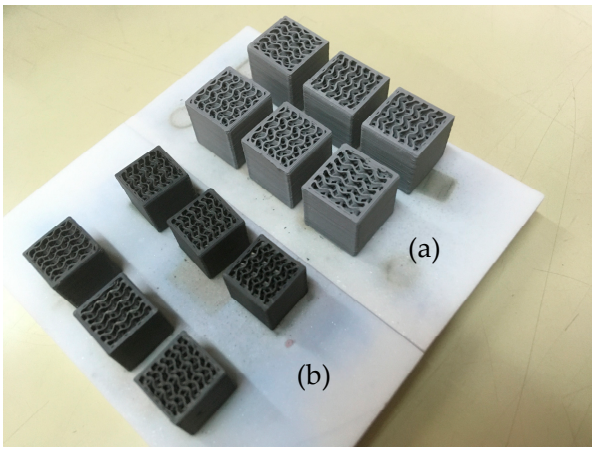

Figure 4. Top view of 3D printed parts before (**a**) and after sintering (**b**).

2.2. Thermal Shock Testing

The thermal shock tests were performed at renewed SF60 [39]. This furnace consists of a flat heliostat, a parabolic concentrator, and a 45° tilted mirror, turning the horizontal optical beam onto a vertical one incident to the sample's holder. The radiant energy was controlled by the angular motion of the shutter slats. An octagonal-shaped secondary concentrator, called a homogenizer, was used to enable a more uniform temperature distribution over all the exposed samples (Figure 5a). The thermal shock cycles were performed using a computer-controlled guillotine system (Figure 5a,b).

Temperature measurements were carried out by a B-type thermocouple placed underneath a flat Black Zirconia plate placed in the middle of the sample holder (control temperature, Figure 5c), together with eight K-type thermocouples placed in touch with the bottom surface of the exposed samples (Figure 5d).

Five thermal shock cycles were undertaken at temperatures ranging from 800 to 1300 °C, corresponding to ΔT of 300, 400, and 500 K. The number of cycles was set at 25, 50, and 100.

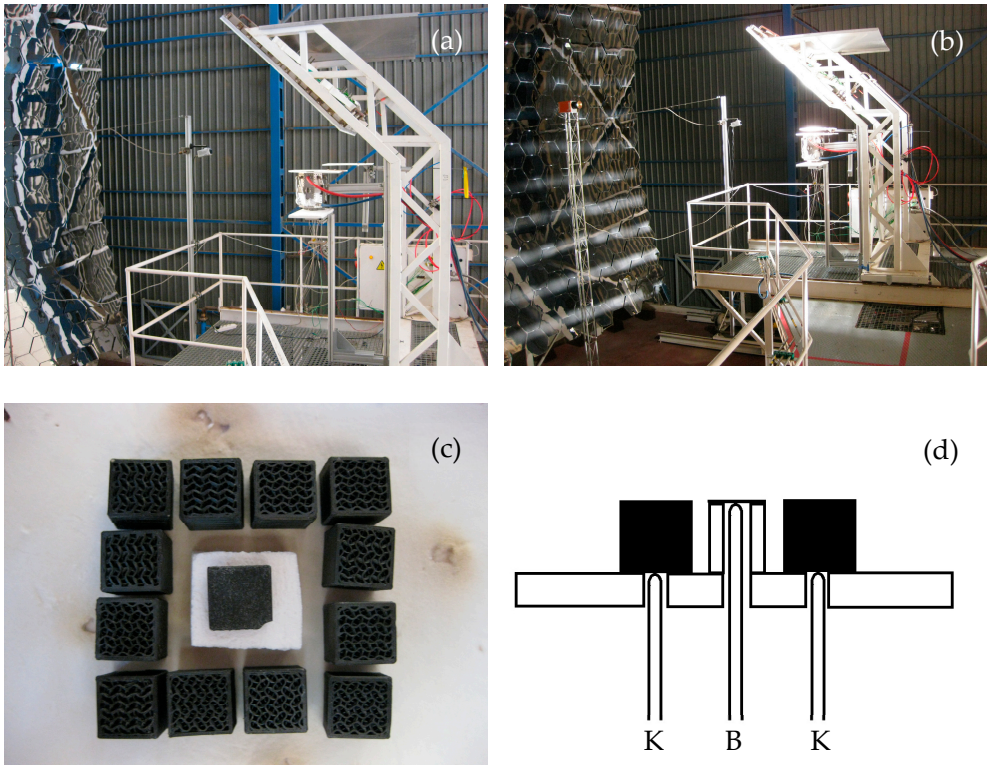

Figure 5. Experimental setup of the guillotine system set on the power ON position (**a**) and power OFF position (**b**), top view of samples (**c**), and scheme of the B- and K-type thermocouples positioning (**d**).

Some of the thermal cycles performed are shown in Figure 6. For each test, the guillotine's on/off cycles were set in a dedicated LabView software, depending on the actual heating and cooling times. For instance, heating time was set at 40 s, whereas cooling time ranged from 28 s to 45 s for ΔT = 300 K and 500 K, respectively. Cooling was carried out under natural conditions.

Thermal shock experiments were also carried out by water quenching followed by measurement of the retained crushing strength, for comparison purposes. The samples were heated at temperatures of 320, 370, and 420 °C. After a dwell time of 60 min, the samples were dipped in water at 20 °C for less than 5 s, corresponding to ΔT of 300, 350, and 400 K, respectively.

2.3. Crushing Testing

The crushing tests were conducted on a mechanical testing machine (Model 4302 Instron Corporation, Canton, MA, USA) using a 10 kN load cell. Closing of the flat steel plates was set at a crosshead speed of 0.5 mm min^{-1} and room temperature [40]. The specimens' cross-sectional areas and the point in the chart curve where a change in slope was observed (inset in Figure 7) were used to determine the value of the nominal load required to calculate the "crushing strength" for each sample. As the surfaces of the samples were not entirely parallel, a compliant 1 mm thick rubber spacer was employed in between the steel plates and the specimens to ensure uniform loading. Four specimens were evaluated in every condition.

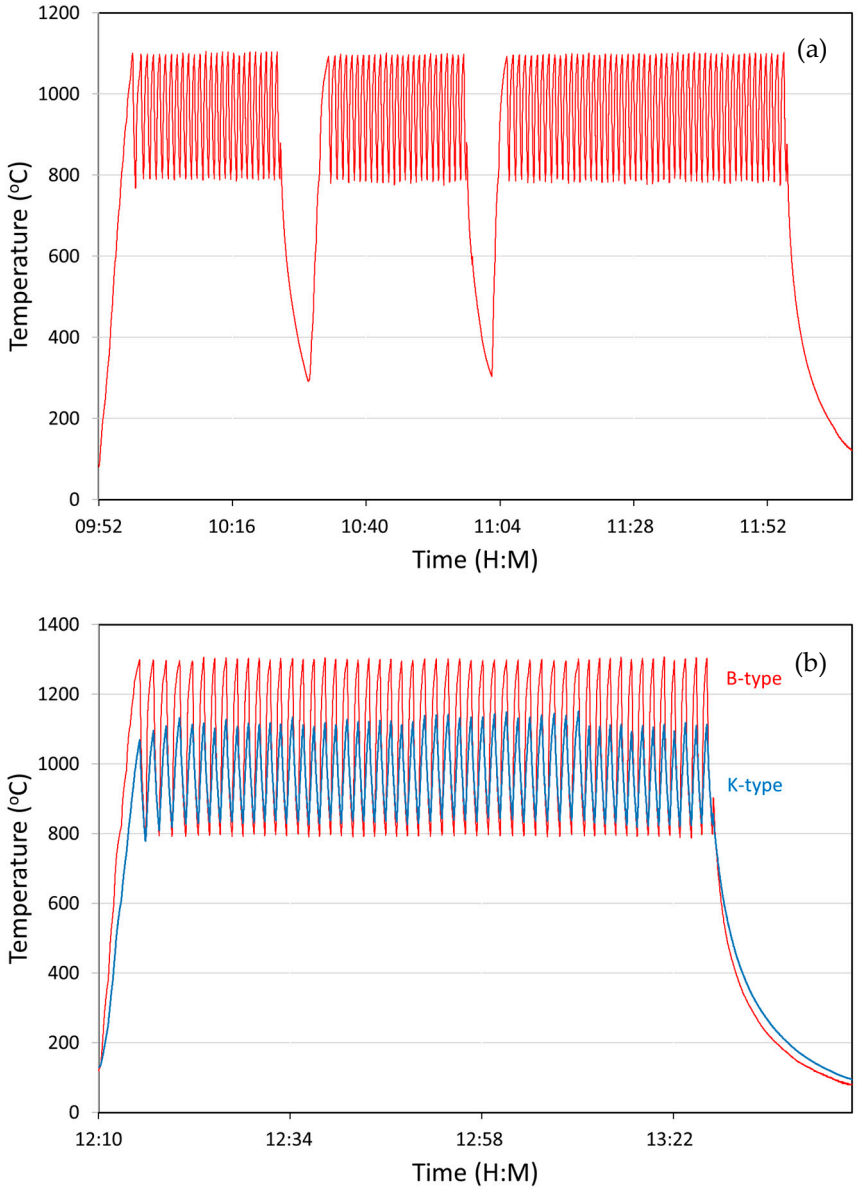

Figure 6. Temperature profiles for ΔT = 300 K (25 + 25 + 50 cycles) using a B-type thermocouple (**a**) and ΔT = 500 K (50 cycles) using B-type and K-type thermocouples (**b**).

3. Results and Discussion

3.1. Materials Characterization

The measured density (Archimedes method) of the 3D-printed Black Zirconia walls was 6.0 ± 0.1 Mg m^{-3}. The core density of the cubes was calculated as 1.4 ± 0.1 Mg m^{-3}, which corresponds to a porosity (P) of around 77%, bearing in mind that P = 1 − (1.4/6.0).

The geometric dimensions of the cubes are listed in Table 1.

Table 1. Mean geometric dimensions (in mm) of the 3D-printed cubes.

	After Printing	After Sintering	Shrinkage (%)
Wall thickness	0.95 ± 0.05	0.76 ± 0.06	20
Strut thickness	0.51 ± 0.04	0.41 ± 0.05	20
Distance between struts	1.53 ± 0.04	1.21 ± 0.04	21

3.2. Thermal Shock Behaviour

Typical crushing strength versus strain curves are shown in Figure 7.

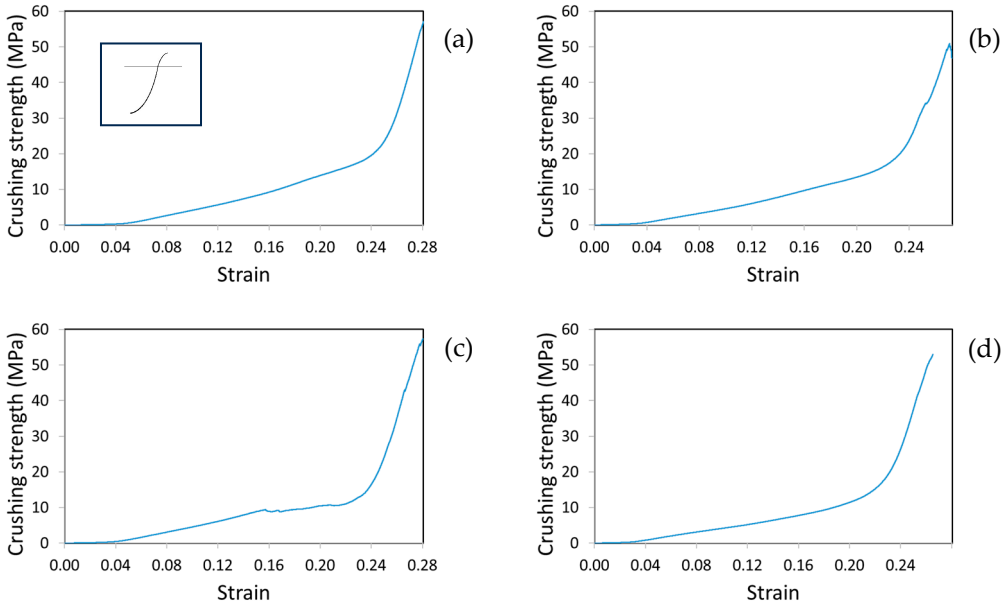

Figure 7. Crushing strength–strain curves for as-sintered (**a**) and ΔT = 300 K, 25 cycles (**b**), 50 cycles (**c**), and 100 cycles (**d**).

The slope increases with increasing strain until a macrocrack starts propagating, which alters the shape of the curve. Therefore, the value where the slope changed was considered as the rupture strength, as illustrated in the inset in Figure 7a. Following an initial onset related to the adjustment, the strength increased more or less in a linear way, as often observed when testing brittle ceramics under tension. The as-sintered crushing strength of the cubes (~35 MPa, see Table 1) is slightly higher than the reported values for silicon carbide foams with a similar total porosity (~75%), typically in the range of 17 to 22 MPa [41,42], which are commonly used as potential candidates for solar receivers.

The mean values of rupture strength (σ_{cs}) are listed in Table 2.

Table 2. Strength data for the various testing conditions.

T Range (°C)	ΔT (K)	No. Cycles	$\sigma_{cs} \pm$ SD (MPa)
-	-	-	35.3 ± 2.2 [1]
800–1100	300	25	32.0 ± 2.3
800–1100	300	50	25.4 ± 2.6
800–1100	300	100	24.2 ± 1.5
800–1200	400	50	21.3 ± 2.7
800–1300	500	50	5.7 ± 1.6
Water quenching			
20–320	300	1	33.5 ± 1.6
20–370	350	1	29.3 ± 1.9
20–420	400	1	23.4 ± 2.3

[1] As-sintered.

For ΔT = 300 K, the retained strength decreased with the increase in the number of cycles, although a small variation was observed from 50 to 100 cycles. A drop of about 10% was observed for ΔT = 300 K after 25 cycles. In turn, a total drop of σ_{cs} of about 31% was determined for 100 cycles. Comparing the data obtained for samples subjected to water quenching, no significant difference in crushing strength is noticed, suggesting that the degree of degradation is closely related to the stresses generated by sudden changes

in temperature during the initial thermal cycle, inducing flaws that propagate at a small pace. This would suggest that after the initial damage imposed onto the material, it holds subsequent cycles with little deterioration.

By increasing the ΔT from 300 to 400 K (50 cycles), the resulting σ_{cs} decreased by about 16%. In total, a drop of around 40% was recorded. This is also in good agreement with data obtained for water quenching under the same temperature difference. According to the ASTM C 1525-04 standard [43], ΔT_c is determined by a reduction in the mean strength of at least 30%. This occurred for ΔT = 300 K after 100 cycles. When ΔT was further increased to 500 K (50 cycles), some macrocracks were visible, and a significant drop (up to 85%) in crushing resistance occurred. Therefore, the maximum thermal stresses that these cubes can withstand fall in the range of 300 to 400 K, depending on the number of thermal cycles. Such a result is in good agreement with data presented by Fargas et al. [44], who showed that no crack propagation was detected in Y-TZP until ΔT was close to 370 °C for a crack generated with an indentation load of 300 N; Riyad et al. obtained similar results [45]. The results gathered in the present work are better than anticipated given the relatively poor thermal shock resistance associated with the moderate K_{Ic} (~4 MPa $m^{1/2}$) [46] and the high thermal expansion coefficient (10.5 × 10^{-6} K in the range of 298 to 1273 K) [47] of YSZ. Still, the σ_{cs} values of samples exposed to ΔT = 400 K for 50 cycles (~21 MPa) are within the range of as-received SiC foams with similar porosity [41,42]. In addition, considering data shown in Figure 6, the difference in temperature between the top and bottom surfaces is around 300 K for ΔT = 500 K, decreasing to 250 K for ΔT = 300 K due to the YSZ low thermal conductivity (3.2 to 2.5 W m^{-1} K^{-1} from 298 to 873 K, respectively) [48]. For the same ΔT, this might explain the fact that the retained crushing strength of the solar-exposed samples is slightly lower than the water-quenched ones. On the other hand, the decrease in density of the 3D-printed cubes ought to increase thermal shock resistance, which also dependent on pore structure, with the extent of damage decreasing with an increase in pore size [49]. Unlike dense ceramic specimens, ceramic foams are less prone to damage produced by thermal shock stresses. Their retained strengths decrease gradually with increasing ΔT, as also observed in the present study [50]. The thermal shock resistance of such 3D-printed Black Zirconia is dependent on the shape and pore size, density, elastic modulus, strength, thermal expansion coefficient, and thermal conductivity. Future work will address the influence of these parameters on improving the thermal behavior of 3D-printed parts.

4. Conclusions

The following conclusions can be drawn from the present work:

(a) The fabrication of 3D-printed highly porous (~77%) Black Zirconia cubes by fused filament fabrication for use in solar receivers was demonstrated. The manufactured specimens were easy to shape and handle.
(b) Starting with the description of the entire fabrication process, the thermal cycling experimental setup suitable for testing these cubes under well-controlled thermal shock conditions by direct exposure to solar radiation was accomplished.
(c) After the thermal cycles, the exposed cubes retained at least 60% of their initial crushing strength at room temperature for ΔT up to 400 K and 50 cycles.
(d) The prepared cubes showed compressive strengths suitable for solar receiver applications (up to 35 MPa) due to the selected geometry.

Author Contributions: Conceptualization, F.A.C.O. and J.C.F.; methodology, M.S., M.L., J.G., J.R. and I.C.; software, M.S. and M.L.; validation, F.A.C.O. and J.C.F.; formal analysis, F.A.C.O., M.S. and J.C.F.; investigation, F.A.C.O., I.C. and J.C.F.; resources, J.C.F.; data curation, F.A.C.O., M.S. and J.C.F.; writing—original draft preparation, F.A.C.O., M.S. and J.C.F.; writing—review and editing, F.A.C.O., M.S., J.G., J.R., I.C., M.L. and J.C.F.; visualization, F.A.C.O., M.S. and J.C.F.; supervision, F.A.C.O. and J.C.F.; project administration, F.A.C.O.; funding acquisition, F.A.C.O., M.S. and J.C.F. All authors have read and agreed to the published version of the manuscript.

Funding: This research was funded by Fundação para a Ciência e a Tecnologia (FCT) through IDMEC under LAETA, grant UIDB/50022/2020. The funding provided by FCT to INIESC, the National Research Infrastructure for Concentrated Solar Energy through contract ALT20-03-0145-FEDER-022113, is also thanked. The funding provided by the European Commission through the SFERA-III project (grant agreement No. 823802) is gratefully acknowledged.

Data Availability Statement: The datasets generated during and/or analyzed during the current study are available from the corresponding author upon reasonable request.

Acknowledgments: We gratefully acknowledge the CIEMAT-PSA Laboratory for providing access to its installations. The administrative support of Marta Ruiz is also appreciated. M.S. gratefully acknowledges FCT for a PhD research grant with reference No. 2021.04919.BD.

Conflicts of Interest: The authors declare no conflict of interest.

References

1. Al-Qutub, A.; Laoui, T.; Zulhazmi, G.; Samad, M.A. Evaluation of durability of alumina, silicon carbide and siliconized silicon carbide foams as absorber materials for concentrated solar power applications. *Sol. Energy* **2022**, *242*, 45–55. [CrossRef]
2. Ávila-Marín, A.L. Volumetric receivers in solar thermal power plants with central receiver system technology: A review. *Sol. Energy* **2011**, *85*, 891–910. [CrossRef]
3. Lidor, A.; Fend, T.; Roeb, M.; Sattler, C. Parametric investigation of a volumetric solar receiver-reactor. *Sol. Energy* **2020**, *204*, 256–269. [CrossRef]
4. Buck, R.; Schwarzbözl, P. Solar tower systems. In *Comprehensive Energy System*; Dincer, I., Ed.; Elsevier: Amsterdam, The Netherlands, 2018; Volume 4, pp. 692–732.
5. Roldán, M.; Smirnova, O.; Fend, T.; Casas, J.; Zarza, E. Thermal analysis and design of a volumetric solar absorber depending on the porosity. *Renew. Energ.* **2014**, *62*, 116–128. [CrossRef]
6. Kribus, A.; Gray, Y.; Grijnevich, M.; Mittelman, G.; Mey-Cloutier, S.; Caliot, C. The promise and challenge of solar volumetric absorbers. *Sol. Energy* **2014**, *110*, 463–481. [CrossRef]
7. Feng, T.; Reutter, O.; Pitz-Paal, R.; Bauer, J. Two novel high-porosity materials as volumetric receivers for concentrated solar radiation. *Solar Energy Mat. Sol. Cells* **2004**, *84*, 291–304.
8. Mey-Cloutier, S.; Caliot, C.; Kribus, A.; Gray, Y.; Flamant, G. Experimental study of ceramic foams used as high temperature volumetric solar absorber. *Sol. Energy* **2016**, *136*, 226–235. [CrossRef]
9. Romero, M.; Buck, R.; Pacheco, J.E. An update on solar central receiver systems, projects, and technologies. *Int. J. Sol. Energy Eng.* **2002**, *124*, 98–108. [CrossRef]
10. Haeger, M.; Keller, L.; Monterreal, R.; Valverde, A. *Phoebus Technology Program Solar Air Receiver (TSA)*; CIEMAT: Madrid, Spain, 1994.
11. Patil, V.R.; Kiener, F.; Grylka, A.; Steinfeld, A. Experimental testing of a solar air cavity- receiver with reticulated porous ceramic absorbers for thermal processing at above 1000 °C. *Sol. Energy* **2021**, *214*, 72–85. [CrossRef]
12. Oliveira, F.A.C.; Fernandes, J.C.; Galindo, J.; Rodríguez, J.; Cañadas, I.; Rosa, L.G. Thermal resistance of solar volumetric absorbers made of mullite, brown alumina and ceria foams under concentrated solar radiation. *Sol. Energy Mater. Sol. Cells* **2019**, *194*, 121–129. [CrossRef]
13. Tofail, S.A.M.; Koumoulos, E.P.; Bandyopadhyay, A.; Bose, S.; O'Donoghue, L.; Charitidis, C. Additive manufacturing: Scientific and technological challenges, market uptake and opportunities. *Mater. Today* **2018**, *21*, 22–37. [CrossRef]
14. Abdulhameed, O.; Al-Ahmari, A.; Ameen, W.; Mian, S.H. Additive manufacturing: Challenges, trends, and applications. *Adv. Mech. Eng.* **2019**, *11*, 1–27. [CrossRef]
15. Vicente, C.M.S.; Sardinha, M.; Reis, L.; Ribeiro, A.; Leite, M. Large-format additive manufacturing of polymer extrusion-based deposition systems: Review and applications. *Prog. Addit. Manuf.* **2023**, 1–24. [CrossRef]
16. Ribeiro, I.; Matos, F.; Jacinto, C.; Salman, H.; Cardeal, G.; Carvalho, H.; Godina, R.; Peças, P. Framework for life cycle sustainability assessment of additive manufacturing. *Sustainability* **2020**, *12*, 929. [CrossRef]
17. Bouzaglou, O.; Golan, O.; Lachman, N. Process design and parameters interaction in material extrusion 3D printing: A review. *Polymers* **2023**, *15*, 2280. [CrossRef]
18. Picard, M.; Mohanty, A.K.; Misra, M. Recent advances in additive manufacturing of engineering thermoplastics: Challenges and opportunities. *RSC Adv.* **2020**, *10*, 36058–36089. [CrossRef]
19. Harshit, K.; Dave, H.K.; Davim, J.P. (Eds.) *Fused Deposition Modeling Based 3D Printing*; Springer: Cham, Switzerland, 2021.
20. Durakbasa, N.M.; Gençyilmaz, M.G. (Eds.) *Digital Conversion on the Way to Industry 40*; Springer Nature Switzerland AG: Basel, Switzerland, 2021.
21. Klocke, F. Modern approaches for the production of ceramic components. *J. Eur. Ceram. Soc.* **1997**, *17*, 457–465. [CrossRef]
22. Gonzalez, H. Challenges in Additive Manufacturing of Alumina. Master's Thesis, University of California, Irvine, CA, USA, 2016.
23. Zocca, A.; Colombo, P.; Gomes, C.M.; Günster, J. Additive manufacturing of ceramics: Issues, potentialities, and opportunities. *J. Am. Ceram. Soc.* **2015**, *98*, 1983–2001. [CrossRef]

24. Deckers, J.; Vleugels, J.; Kruth, J.P. Additive manufacturing of ceramics: A review. *J. Ceram. Sci. Technol.* **2014**, *5*, 245–260.
25. Lakhdar, Y.; Tuck, C.; Binner, J.; Terry, A.; Goodridge, R. Additive manufacturing of advanced ceramic materials. *Prog. Mater. Sci.* **2021**, *116*, 100736. [CrossRef]
26. Gao, S.; Wang, C.; Zhao, Z. Mechanical properties of ZrO_2 honeycomb sandwich structures by 3D printing. *IOP Conf. Ser. Mater. Sci. Eng.* **2019**, *678*, 012018. [CrossRef]
27. Veteška, P.; Hajdúchová, Z.; Feranc, J.; Tomanová, K.; Milde, J.; Kritikos, M.; Bača, L.; Janek, M. Novel composite filament usable in low-cost 3D printers for fabrication of complex ceramic shapes. *Appl. Mater. Today* **2021**, *22*, 100949. [CrossRef]
28. Guan, Z.; Yang, X.; Liu, P.; Xu, X.; Li, Y.; Yang, X. Additive manufacturing of zirconia ceramic by fused filament fabrication. *Ceram. Int.* **2023**, *49*, 27742–27749. [CrossRef]
29. Smirnov, A.; Kuznetsova, E.V.; Babushkin, N.N.; Pristinskiy, Y.O.; Solis Pinargote, N.W. Rheological properties of powder blend for extrusion of ceramic-polymer filament used in 3D printing. *Int. J. Phys. Conf. Ser.* **2021**, *2144*, 012005. [CrossRef]
30. Nötzel, D.; Eickhoff, R.; Pfeifer, C.; Hanemann, T. Printing of zirconia parts via fused filament fabrication. *Materials* **2021**, *14*, 5467. [CrossRef] [PubMed]
31. Nötzel, D.; Hanemann, T. New feedstock system for fused filament fabrication of sintered alumina parts. *Materials* **2020**, *13*, 4461. [CrossRef] [PubMed]
32. Cano, S.; Gonzalez-Gutierrez, J.; Sapkota, J.; Spoerk, M.; Arbeiter, F.; Schuschnigg, S.; Holzer, C.; Kukla, C. Additive manufacturing of zirconia parts by fused filament fabrication and solvent debinding: Selection of binder formulation. *Addit. Manuf.* **2019**, *26*, 117–128. [CrossRef]
33. Orlovská, M.; Hain, M.; Kitzmantel, M.; Veteška, P.; Hajdúchová, Z.; Janek, M.; Vozárová, M.; Bača, L. Monitoring of critical processing steps during the production of high dense 3D alumina parts using fused filament fabrication technology. *Addit. Manuf.* **2021**, *48 Pt A*, 102395. [CrossRef]
34. Truxová, V.; Šafka, J.; Sobotka, J.; Macháček, J.; Ackermann, M. Alumina manufactured by fused filament fabrication: A comprehensive study of mechanical properties and porosity. *Polymers* **2022**, *14*, 991. [CrossRef]
35. Schlacher, J.; Hofer, A.-K.; Geier, S.; Kraleva, I.; Papšík, R.; Schwentenwein, M.; Bermejo, R. Additive manufacturing of high-strength alumina through a multi-material approach. *Open Ceram.* **2021**, *5*, 100082. [CrossRef]
36. Cano, S.; Lube, T.; Huber, P.; Gallego, A.; Naranjo, J.A.; Berges, C.; Schuschnigg, S.; Herranz, G.; Kukla, C.; Holzer, C.; et al. Influence of the Infill Orientation on the Properties of Zirconia Parts Produced by Fused Filament Fabrication. *Materials* **2020**, *13*, 3158.
37. Black Zirconia Zetamix Filament. Available online: https://zetamix.fr/en/produit/black-zirconia-zetamix-filament/ (accessed on 30 June 2023).
38. Design Guide—Black Zirconia. Available online: https://zetamix.fr/wp-content/uploads/2023/03/Design-Guide-Black-Zirconia.pdf (accessed on 30 June 2023).
39. Rodríguez, J.; Cañadas, I.; Monterreal, R.; Enrique, R.; Galindo, J. PSA SF60 solar furnace renewed. In Proceedings of the SolarPACES 2018: International Conference on Concentrating Solar Power and Chemical Energy Systems, Casablanca, Morocco, 2–5 October 2018. [CrossRef]
40. Oliveira, F.A.C.; Dias, S.; Vaz, M.F.; Fernandes, J.C. Behaviour of open-cell cordierite foams under compression. *J. Eur. Ceram. Soc.* **2006**, *26*, 179–186. [CrossRef]
41. Tian, C.; Zhang, J.; Cao, X.; Liu, Q.; Hu, W. High strength silicon carbide foams and their deformation behavior. *J. Mater. Sci. Technol.* **2006**, *22*, 269–272.
42. Eom, J.-H.; Kim, Y.-W.; Park, C.B.; Wang, C. Effect of forming methods on porosity and compressive strength of polysiloxane-derived porous silicon carbide ceramics. *J. Ceram. Soc. Jpn.* **2012**, *120*, 199–203. [CrossRef]
43. *ASTM C 1525-04*; Standard Test Method for Determination of Thermal Shock Resistance for Advanced Ceramics by Water Quenching. ASTM International: West Conshohocken, PA, USA, 2004.
44. Fargas, G.; Casellas, D.; Llanes, L.; Anglada, M. Thermal shock resistance of yttria-stabilized zirconia with Palmqvist indentation cracks. *J. Eur. Ceram. Soc.* **2003**, *23*, 107–114. [CrossRef]
45. Riyad, M.F.; Mahmoudi, M.; Minary-Jolandan, M. Manufacturing and thermal shock characterization of porous yttria stabilized zirconia for hydrogen energy systems. *Ceramics* **2022**, *5*, 472–483. [CrossRef]
46. Casellas, D.; Llanes, L.; Cumbrera, F.; Sánchez-Bajo, F.; Forsling, W.; Anglada, M. On the transformation toughening of Y-ZrO_2 ceramics with mixed TZP/PSZ microstructures. *J. Eur. Ceram. Soc.* **2001**, *21*, 147–159. [CrossRef]
47. Yasuda, I.; Hishinuma, M. Lattice expansion of acceptor-doped lanthanum chromites under high-temperature reducing atmospheres. *Electrochemistry* **2000**, *68*, 526–530. [CrossRef]
48. Hasselman, D.P.H.; Johnson, L.F.; Bentsen, L.D.; Syed, R.; Lee, H.L.; Swain, M.V. Thermal diffusivity and conductivity of dense polycrystalline ZrO_2 ceramics: A survey. *Am. Ceram. Soc. Bull.* **1987**, *66*, 799–806.
49. Vedula, V.R.; Green, D.J.; Hellman, J.R. Thermal shock resistance of ceramic foams. *J. Am. Ceram. Soc.* **1999**, *82*, 649–656. [CrossRef]
50. Oliveira FA, C.; Dias, S.; Fernandes, J.C. Thermal Shock Behaviour of Open-Cell Cordierite Foams. In *Materials Science Forum*; Trans Tech Publications, Ltd.: Zurich, Switzerland, 2006; Volume 514–516, pp. 764–767.